

# Selective autophagy associated with iron overload aggravates non-alcoholic steatohepatitis via ferroptosis

Koki Honma<sup>1</sup>, Sora Kirihara<sup>1</sup>, Hinako Nakayama<sup>1</sup>, Taketo Fukuoka<sup>1</sup>, Toshiaki Ohara<sup>2</sup>, Kazuya Kitamori<sup>3</sup>, Ikumi Sato<sup>4</sup>, Satoshi Hirohata<sup>4</sup>, Moe Fujii<sup>5</sup>, Shusei Yamamoto<sup>1,4</sup>, Shang Ran<sup>6</sup> and Shogo Watanabe<sup>4</sup> 

<sup>1</sup>Department of Medical Technology, Graduate School of Health Sciences, Okayama University, Okayama 700-8558, Japan;

<sup>2</sup>Department of Pathology and Experimental Medicine, Graduate School of Medicine, Dentistry and Pharmaceutical Science, Okayama University, Okayama 700-8558, Japan; <sup>3</sup>College of Human Life and Environment, Kinjo Gakuin University, Nagoya 463-8521, Japan;

<sup>4</sup>Academic Field of Health Science, Okayama University, Okayama 700-8558, Japan; <sup>5</sup>Department of Medical Technology, Ehime Prefectural University of Health Sciences, Ehime 791-2101, Japan; <sup>6</sup>HeiLongjiang Provincial Center for disease control and prevention, Harbin 150030, China

Corresponding author: Shogo Watanabe. Email: watanabe1224@okayama-u.ac.jp

## Impact Statement

Iron overload is frequently observed in non-alcoholic steatohepatitis (NASH), and the amount of iron in the liver positively correlates with the histological severity of NASH. However, the mechanism of iron overload aggravates NASH remains unclear. Ferroptosis, a novel form of iron-dependent cell death, is closely related to autophagy. In this study, we first demonstrated that iron overload induces ferroptosis via autophagy and aggravates NASH using NASH rodent model. In rats in which iron levels were elevated, selective autophagy (ferritinophagy, lipophagy) and ferroptosis were accelerated and aggravated NASH. This study indicates that selective autophagy, which contributes to the homeostasis of the body, may exacerbate NASH and can lead to the translational research to explore new therapeutic strategies for NASH.

## Abstract

Non-alcoholic steatohepatitis (NASH) is a progressive form of non-alcoholic fatty liver disease (NAFLD) that causes cirrhosis and hepatocellular carcinoma. Iron is an essential trace element in the body; however, excess iron can cause tissue damage and dysfunction. Iron overload is often observed in patients with NASH, and the amount of iron accumulated in the liver positively correlates with the histological severity of NASH. Ferroptosis, a novel form of iron-dependent cell death, is caused by the accumulation of lipid peroxidation and oxidative stress and is related to NASH. In addition, ferroptosis is closely related to autophagy, an intracellular self-degradation process. Although autophagy has many beneficial effects, it may also be harmful to the organism, for example, inducing ferroptosis. It is unclear whether iron overload aggravates NASH via autophagy. The aim of this research is to determine the mechanism by which iron overload induces ferroptosis via autophagy and aggravates NASH. Stroke-prone spontaneously hypertensive rats (SHRSP5/Dmcr) were divided into two groups and fed a high-fat and high-cholesterol (HFC) diet for eight weeks. Iron dextran was administered to the Fe group in addition to the HFC diet. Blood analysis, histological staining, calcineurin activity assay, quantitative reverse transcription polymerase chain reaction (RT-PCR), immunofluorescence staining, and electron microscopy were performed. The results showed that iron overload promoted autophagy via nuclear translocation of transcription factor EB

(TFEB) and induced ferritinophagy, which is the autophagic degradation of ferritin. In addition, the HFC diet induced lipophagy, the autophagic degradation of lipid droplets. The Fe group also exhibited promoted ferroptosis and aggravated hepatic inflammation and fibrosis. In conclusion, iron overload accelerates ferritinophagy and lipophagy, aggravating NASH pathology via ferroptosis. These findings indicate the therapeutic potential of inhibiting autophagy and ferroptosis for treating NASH.

**Keywords:** Non-alcoholic steatohepatitis, ferroptosis, ferritinophagy, lipophagy, autophagy, iron overload

**Experimental Biology and Medicine 2023; 248: 1112–1123. DOI: 10.1177/15353702231191197**

## Introduction

Non-alcoholic fatty liver disease (NAFLD) is a general term for fatty liver disease caused by factors other than alcohol and drugs, such as overeating, stress, and smoking and

has a worldwide prevalence of approximately 25%.<sup>1</sup> Non-alcoholic steatohepatitis (NASH) is a progressive form of NAFLD that involves fibrosis as well as fatty liver, and approximately 7–25% of NASH cases progress to cirrhosis and hepatocellular carcinoma within 10 years.<sup>2</sup> Most NASH

patients present with lifestyle-related diseases, including high blood pressure, lipid disorders, and diabetes, which are aggravating factors of NASH. However, the pathogenesis of NASH remains poorly understood, and there is an urgent need to identify the underlying mechanisms.

Iron is an essential trace element in the body; however, excess iron accumulates in the liver, heart, and endocrine organs, causing tissue damage and dysfunction. Patients with NAFLD/NASH have elevated serum iron and ferritin levels, with approximately one-third of patients showing iron deposition in the liver, the amount of which positively correlates with the histological severity of NASH.<sup>3,4</sup> The body's iron balance is regulated by "hepcidin," a 25 amino-acid peptide that inhibits iron uptake in the gut and iron recycling from macrophages, decreasing the plasma iron levels. Inappropriately low hepcidin synthesis has been reported in NAFLD/NASH, which could facilitate iron uptake and predispose patients to iron overload.<sup>5</sup> In addition, ferroptosis is a novel iron-dependent form of cell death caused by elevated lipid peroxidation and oxidative stress.<sup>6</sup> Ferroptosis is characterized by a reduction/loss of mitochondrial cristae and mitochondrial contraction and differs morphologically, biochemically, and genetically from the other known forms of cell death, such as apoptosis and necrosis. Ferroptosis is closely related to many diseases, including cancer and neurological diseases, and is also associated with the aggravation of NASH pathology.<sup>7,8</sup> However, the detailed mechanism of iron overload-induced ferroptosis remains unclear.

Autophagy is an essential intracellular self-degradation mechanism that degrades abnormal proteins and over-abundant or damaged organelles and can be divided into three categories by the manner of degradation: macroautophagy, microautophagy, and chaperone-mediated autophagy.<sup>9,10</sup> In macroautophagy (hereafter referred to as autophagy), the degradation targets are ingested by isolation membrane, termed the autophagosomes. These autophagosomes fuse with lysosomes to form autolysosomes, whose contents are degraded by lysosome hydrolytic enzymes. Autophagy can occur via non-selective or selective pathways for the removal of specific organelles.<sup>11–13</sup> Selective autophagy plays an important role in intracellular homeostasis; however, it may also produce degradation products that are harmful to the organism, for example, inducing ferroptosis.<sup>14,15</sup>

In this study, we used a stroke-prone (SP) spontaneously hypertensive rat model (SHRSP5/Dmcr) to examine the mechanism by which iron overload induces ferroptosis via selective autophagy and aggravates NASH.

## Materials and methods

### Animal models and diets

Male SHRSP5/Dmcr rats (9-week-old) were obtained from the Disease Model Cooperative Research Association (Kyoto, Japan). The SHRSP5/Dmcr rats developed NASH pathology similar to that of human patients when fed a high-fat and high-cholesterol (HFC) diet.<sup>16</sup> The rats were fed *ad libitum* with water and an SP diet for the first week and allowed to acclimatize to the environment. SP and HFC diets were obtained from Funabashi Farm (Chiba,

Japan; Supplementary Table 1). The rats were divided into two groups at 10 weeks of age: SHRSP5/Dmcr rats + HFC diet (Cont group,  $n=5$ ) and SHRSP5/Dmcr rats + HFC diet + iron dextran (Fe group,  $n=5$ ). Iron dextran (Kyoritsu Seiyaku Co., Ltd., Tokyo, Japan) was administered intraperitoneally (100 mg/kg) three times a week from 10 to 18 weeks of age. Food was provided such that there was no significant difference in the total food intake. HFC loading for eight weeks was sufficient to induce NASH. HFC diet loading for six weeks showed only partial fibrosis in the liver; however, at eight weeks, fibrosis was observed throughout the liver.<sup>17</sup> Body weight was measured weekly from 10 to 18 weeks of age.

All the rat experiments were treated in strict accordance with the recommendations of the standard of Care and Management of Laboratory Animals and Relief of Pain published by the Japanese Ministry of Environment (2006). This study was approved by the Animal Experiment Committee of Okayama University (approval no. OKU-2021207).

### Blood and organ analysis

At 18 weeks of age, the rats were food-deprived overnight, and blood was drawn from the right carotid artery of all rats under anesthesia with pentobarbital sodium (48.6 mg/kg, Nacalai Tesque Inc., Kyoto, Japan). The blood samples were centrifuged at 2500 rpm for 20 min at 4°C, and the sera were stored at –80°C. Aspartate aminotransferase (AST), alanine aminotransferase (ALT), free fatty acid (FFA), triglyceride (TG), iron, total iron-binding capacity (TIBC), and transferrin levels were measured using routine laboratory methods (SRL Inc., Tokyo, Japan). Transferrin saturation (TSAT), an index based on both serum iron and its main transport protein, was calculated using the following formula: TSAT (%) = serum iron (μg/dL)/TIBC (μg/dL) × 100. Serum ferritin levels were measured using a Rat Ferritin ELISA Kit (Immunology Consultants Laboratory Inc., Portland, OR, USA). The liver was excised and weighed, and a portion was sectioned for histopathological staining. The remaining portion was frozen and stored at –80°C for genetic analysis.

### Histopathological analysis of the liver

The livers were fixed in 10% formalin (Kenei Pharmaceutical Co., Ltd., Osaka, Japan) for 48 h, paraffin-embedded, and sliced into 4 μm sections for histological analysis. The sections were stained with Masson's trichrome staining to evaluate fibrosis and Berlin blue staining for iron detection. The NAFLD activity score (NAS) was calculated according to the NASH Clinical Research Network scoring system,<sup>18</sup> which has been adapted to HFC diet-fed rats.<sup>19</sup> An NAS value ≥5 was defined as NASH. Fibrosis was evaluated on a scale of 0–6 using the Ishak stage.<sup>20,21</sup> All images were obtained using the BZ-X700 All-in-One fluorescence microscope (Keyence, Osaka, Japan).

### Calcineurin activity

Calcineurin activity was measured using a Calcineurin Cellular Activity Assay Kit (Enzo Life Science Inc., Farmingdale, NY, USA). Calcineurin activity is specifically

inhibited by ethylene glycol tetraacetic acid (EGTA).<sup>22</sup> The kit is based on a colorimetric method for measuring calcineurin activity in cellular extracts by the amount of phosphate released in the presence/absence of EGTA buffer. Cryopreserved liver samples (100 mg) were homogenized in 500  $\mu$ L of lysis buffer containing protease inhibitors. The samples were then centrifuged (100k  $\times$ g, 4°C, 45 min), and the high-speed supernatant (HSS) was collected. Excess phosphates were removed from the HSS using a chromatographic column, and the supernatant was then used for the assay. Wells corresponding to the background, total phosphatase activity, and EGTA buffer were prepared. RII phosphorylated peptide substrate was added to each well and equilibrated at 30°C for 10 min. The extract (5  $\mu$ L, containing 5 mg/mL protein) was then added to the wells and incubated at 30°C for 30 min. Following incubation, malachite green reagent, a phosphate indicator, was added to the wells, and the absorbance was measured at 620 nm. Measurements were performed on a FlexStation<sup>®</sup> 3 multimode microplate reader (Molecular Devices, Sunnyvale, CA, USA). The concentration of calcineurin in the samples was calculated based on a standard curve.

### Immunofluorescent staining

Immunofluorescent staining was performed to detect 4-hydroxynonenal (4-HNE, a lipid peroxidation byproduct and marker of oxidative stress)<sup>23,24</sup> and transcription factor EB (TFEB, an autophagy-promoting factor). Paraffin-embedded liver samples were sliced into 4  $\mu$ m. Following deparaffinization, antigen retrieval was performed by heating the sections in antigen activation solution (pH 9.0) at 95°C for 20 min. Anti-4-Hydroxynonenal antibody (Abcam plc., Cambridge, UK) and anti-TFEB antibody (Proteintech Group Inc., Chicago, IL, USA) were used as primary antibodies. The sections were incubated with anti-4-HNE antibody overnight at 4°C (colored red using Cyanine 3) and anti-TFEB antibody at room temperature (20–25°C) for 60 min and colored green using fluorescein. The nuclei were simultaneously stained with 4',6-diamidino-2-phenylindole (DAPI). All the processes were performed by Morphotechnology Co., Ltd. (Hokkaido, Japan). The images were analyzed using a BZ-X700 All-in-One fluorescence microscope (Keyence). Analyses of the 4-HNE immunofluorescent areas were performed using digital image processing software (ImageJ; National Institute of Health, Bethesda, MD, USA).

### Mitochondrial morphology analysis

The morphology of the hepatic mitochondria was observed using transmission electron microscopy (TEM; H-7650, Hitachi High-Tech Co., Ltd., Tokyo, Japan). The livers were cut the size of small pieces and prefixed in glutaraldehyde (2%) and paraformaldehyde (2%) overnight at 4°C. After washing with phosphate buffer (pH 7.4, 0.1 M), postfixation was performed with 2% osmium tetroxide (90 min). Washing with phosphate buffer, the tissues were dehydrated and embedded in Spurr, a low-viscosity resin. After thermal polymerization, the livers were sliced into 80 nm ultrathin sections using an ultramicrotome (Leica EM UC7 type, Leica

Microsystems, Wetzlar, Germany). The sections were double-stained with uranium and lead to observe the mitochondrial morphology. The mitochondrial cross-sectional areas were measured from the images, and the mitochondrial sizes were evaluated.

### Quantitative reverse transcription-polymerase chain reaction analysis

Total RNA was isolated from the liver (30 mg) using an RNeasy Mini Kit (Qiagen, Hilden, Germany). The isolated RNA (1000 ng) was subjected to reverse transcription (RT) using the PrimeScript<sup>™</sup> RT Reagent Kit (Takara Bio Inc., Shiga, Japan). Quantitative polymerase chain reaction (PCR) analysis was performed using PowerTrack<sup>™</sup> SYBR<sup>™</sup> Green Master Mix (Thermo Fisher Scientific K.K., Tokyo, Japan) and a StepOnePlus Real-Time PCR System (Thermo Fisher Scientific K.K.). Glyceraldehyde 3-phosphate dehydrogenase (GAPDH) was used as an internal standard. Table 1 shows the sequences of the primers used in the experiments.

### Statistical analysis

Relevant data are expressed as mean value  $\pm$  standard error of mean (SEM). Statistical analysis was performed using the Mann–Whitney *U*-test. Statistical significance was set at  $P < 0.05$ .

## Results

### Physiological data

The total food intake by the two groups was maintained at almost the same level (Figure 1(A)). Significant weight loss was observed in the Fe group compared to that in the Cont group after 15 weeks of age (Figure 1(B)).

### Histological analysis of the liver and biochemical data

Macroscopic analysis revealed marked differences in the liver between the Cont and Fe groups. The liver in the Fe group was yellow-brown and enlarged (Figure 2(A)). In addition, weight of the liver was significantly higher in the Fe group than in the Cont group (Figure 2(D)). Masson's trichrome staining revealed numerous black deposits of iron accumulation and expansion of the fibrotic areas in the Fe group (Figure 2(B) and (C)). The mean serum AST and ALT levels increased in the Fe group, although the differences were not statistically significant (Table 2). NAS showed no significant differences in steatosis grade or hepatocyte ballooning; however, lobular inflammation was significantly increased in the Fe group (Figure 2(E to G)). The NAS scores were  $>5$  points in both groups, indicating NASH but not a significant difference (Figure 2(H),  $P = 0.063$ ). The Ishak fibrosis stage was significantly higher in the Fe group than in the Cont group (Figure 2(I)). The serum FFA level in the Fe group was significantly increased than that in the Cont group. The TG levels were almost the same in both groups (Table 2).

**Table 1.** Primer sequences used in mRNA quantitation by reverse transcription-polymerase chain reaction.

Gene name	Primer	GenBank accession number
Glutathione peroxidase 4 ( <i>GPX4</i> )	F: 5'-TCCATGCACGAATTCGCAGC-3' R: 5'-TCGTA AACCCACTCGGCGT-3'	NM_001039849
Superoxide dismutase 2 ( <i>SOD2</i> )	F: 5'-GAGAAGTACCACGAGGCGCT-3' R: 5'-GCGGCAATCTGTAAGCGACC-3'	NM_017051
Arachidonate 15-lipoxygenase ( <i>ALOX15</i> )	F: 5'-TGGGCCACTGCTGTTCTGTA-3' R: 5'-CCAGTTGCCCCACCTGTACA-3'	NM_031010
Cyclooxygenase 2 ( <i>COX2</i> )	F: 5'-GCTGATGACTGCCAACTC-3' R: 5'-CGGGATGA ACTCTCTCTCA-3'	NM_080591
Monocyte chemotactic protein 1 ( <i>MCP1</i> )	F: 5'-CAGATCTCTTCTCCACC ACTAT-3' R: 5'-CAGGCAGCAACTGTGAACAAC-3'	NM_031530
Tumor necrosis factor- $\alpha$ ( <i>TNF-<math>\alpha</math></i> )	F: 5'-ACTGA ACTTCGGGGTGATTG-3' R: 5'-GCTTGGTGGTTTGCTACGAC-3'	NM_012675
Lysosome-associated membrane protein 2 ( <i>LAMP2</i> )	F: 5'-ATCACGATGCGCCTCCTCTC-3' R: 5'-AAGCTTG CAGGTGAATGCC-3'	NM_017068
Transient receptor potential cation channel, mucolipin subfamily, member 1 ( <i>TRPML1</i> )	F: 5'-CGCTCGCTGTCCATGGTTTC-3' R: 5'-TAACAGCCACCCTCCATGCC-3'	NM_001105903
CLN3 lysosomal/endosomal transmembrane protein, battenin ( <i>CLN3</i> )	F: 5'-CGTTGATCCCACCTGTCCCA-3' R: 5'-GCTGGCCAAAACCACTCCAC-3'	NM_001006971
Unc-51 like autophagy activating kinase 1 ( <i>ULK1</i> )	F: 5'-TGGAGCAAGAGCACACGGAA-3' R: 5'-TGGTCCGTGAGAGTGTGCTG-3'	NM_001108341
UV radiation resistance-associated gene ( <i>UVRAG</i> )	F: 5'-GGAGTGCACCGCCAAAAGAG-3' R: 5'-CATCTGCACCCCGAAACGTG-3'	NM_001401542
Autophagy-related gene 14 ( <i>ATG14</i> )	F: 5'-CGCGACCGGAGAGGTTTAT-3' R: 5'-CTGATCCAAGGGCCCGTGAT-3'	NM_001107258
Nuclear receptor co-activator 4 ( <i>NCOA4</i> )	F: 5'-AGCTGCATTAGTCGCCACT-3' R: 5'-TTTGGGGTGAGCCAGTCTG-3'	NM_001034008
Member of the RAS oncogene family ( <i>Rab10</i> )	F: 5'-ACAGCAGGCCAGGAACGATT-3' R: 5'-AGTCCGCAAGCAGTCACAGA-3'	NM_017359
Dynamin 2 ( <i>DNM2</i> )	F: 5'-GAAGAGCTCATCCGCTGGT-3' R: 5'-GACGGCAAGAATGAGGCTGC-3'	NM_013199
Glyceraldehyde 3-phosphate dehydrogenase ( <i>GAPDH</i> )	F: 5'-TCAAGAAGGTGGTGAAGCAG-3' R: 5'-AGGTGGAAGAATGGGAGTTG-3'	NM_017008

F: forward; R: reverse.

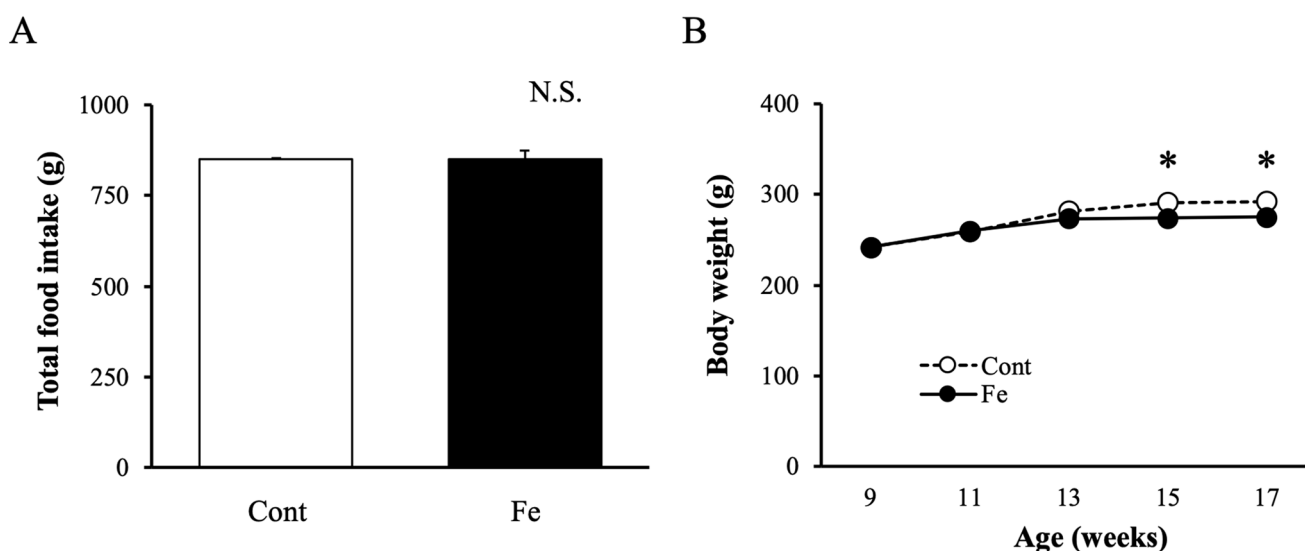


**Figure 1.** Physiological data. (A) Total food intake from 10 to 18 weeks of age. (B) Body weight changes from 10 to 18 weeks of age. All data are shown as the mean value  $\pm$  SE;  $n=5$  in both groups. SE: standard error. \* $P < 0.05$  vs Cont group.

### Iron metabolism

The serum levels of iron, ferritin, and TIBC were significantly higher in the Fe group than those in the Cont group, whereas transferrin was significantly lower in the Fe group than that in

the Cont group (Table 2 and Figure 3(A)). TSAT, an iron content index, was significantly higher in the Fe group than that in the Cont group (Table 2). Berlin blue staining revealed numerous iron deposits in the liver in the Fe group (Figure 3(B) and (C)).

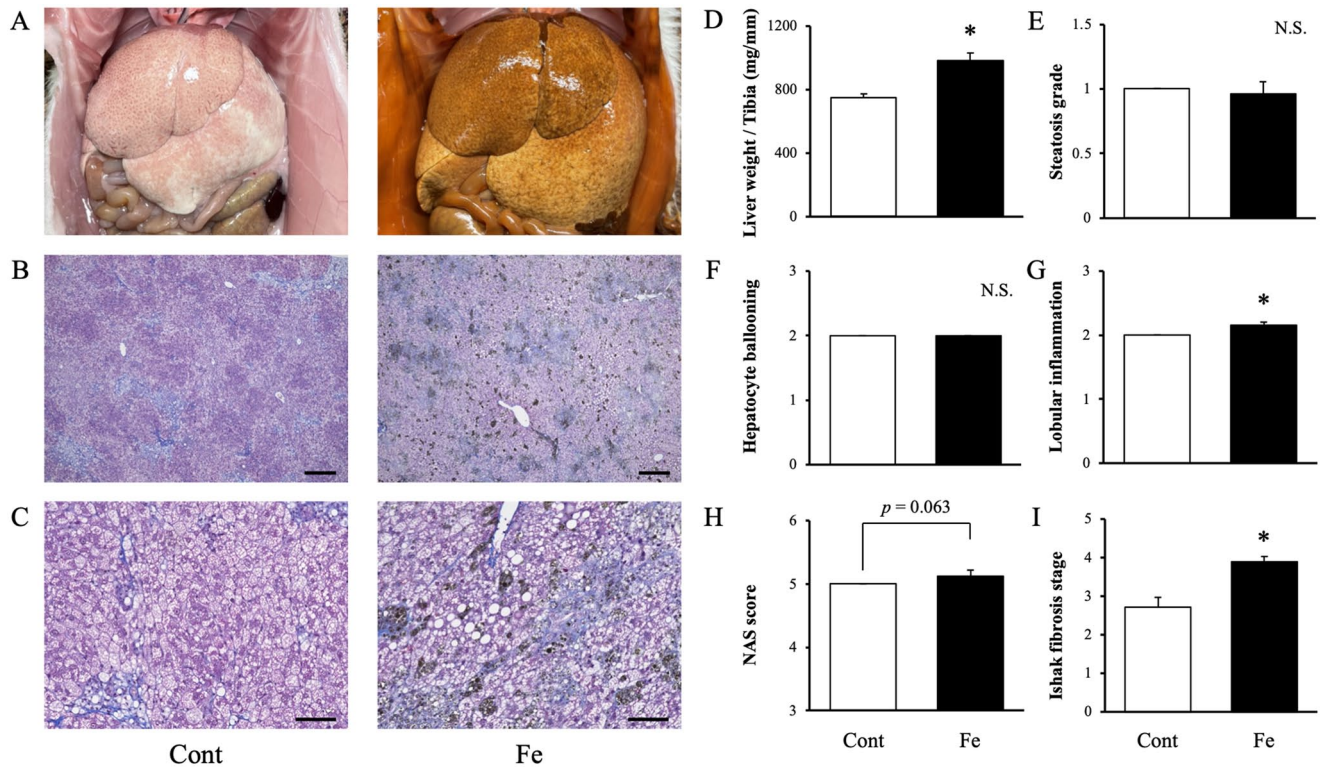


**Figure 2.** Histological analysis of the liver. (A) Macroscopic finding in the liver. (B) and (C) Masson trichrome staining of hepatic fibrosis (B: scale bar = 400  $\mu$ m, C: scale bar = 100  $\mu$ m). (D) Liver weight corrected by tibia length. (E) Steatosis grade. (F) Hepatocyte ballooning. (G) Lobular inflammation. (H) NAS score. (I) The Ishak fibrosis stage. All data are shown as the mean value  $\pm$  SE;  $n=5$  in both groups.

NAS: NAFLD activity score; NAFLD: non-alcoholic fatty liver disease; SE: standard error.

\* $P < 0.05$  vs Cont group.

**Table 2.** The results of biochemical analysis in serum at 18 weeks of age.

Parameters	Cont	Fe	Normal range <sup>a</sup>
AST (IU/L)	204.8 $\pm$ 7.7	221.8 $\pm$ 26.1	98.2 $\pm$ 6.7
ALT (IU/L)	131.2 $\pm$ 7.7	145.2 $\pm$ 12.7	50.1 $\pm$ 4.3
FFA ( $\mu$ EQ/L)	440.4 $\pm$ 50.8	829 $\pm$ 83.5*	421.3 $\pm$ 42.9
TG (mg/dL)	6.2 $\pm$ 1.9	5.8 $\pm$ 1.8	5.2 $\pm$ 1.4
Iron ( $\mu$ g/dL)	87.6 $\pm$ 5.8	823.6 $\pm$ 111.2*	81.6 $\pm$ 7.1
TIBC ( $\mu$ g/dL)	510.6 $\pm$ 11.4	860.4 $\pm$ 132.1*	500.1 $\pm$ 12.8
Transferrin (mg/dL)	139.2 $\pm$ 2.1	123.4 $\pm$ 2.0*	143.6 $\pm$ 5.2
TSAT (rate)	17.1 $\pm$ 0.8	96.6 $\pm$ 2.1*	16.3 $\pm$ 0.9

AST: aspartate aminotransferase; ALT: alanine aminotransferase; FFA: free fatty acid; TG: triglyceride; TIBC: total iron-binding capacity; TSAT: transferrin saturation; TSAT (%) = iron ( $\mu$ g/dL)/TIBC ( $\mu$ g/dL)  $\times$  100.

All data are shown as mean value  $\pm$  standard error (SEM);  $n=5$  in both groups.

<sup>a</sup>Biochemical data for SHRSP5/Dmcr rats fed a normal (SP) diet for eight weeks are shown for reference in the normal range.

\* $P < 0.05$  vs Control group.

### Hepatic calcineurin activity and immunofluorescence staining of TFEB

Calcineurin activity in the liver was significantly higher in the Fe group than in the Cont group (Figure 4(A)). Immunofluorescence staining of TFEB revealed marked differences between the Cont and Fe groups. TFEB was confined to the cytoplasm and undetectable in the nucleus in the Cont group. In contrast, most of the TFEB in the Fe group was detectable in the nucleus (Figure 4(B)).

### Oxidative stress and inflammation markers

The mRNA expression of the antioxidative response enzymes glutathione peroxidase 4 (*GPX4*) and superoxide dismutase 2 (*SOD2*) was significantly downregulated in the Fe group compared to that in the Cont group (Figure 5(A)). In contrast, the mRNA expression of the oxidative response enzymes arachidonate 15-lipoxygenase (*ALOX15*) and cyclooxygenase 2 (*COX2*) was significantly upregulated in the Fe group (Figure 5(B)). In addition, the inflammatory markers,

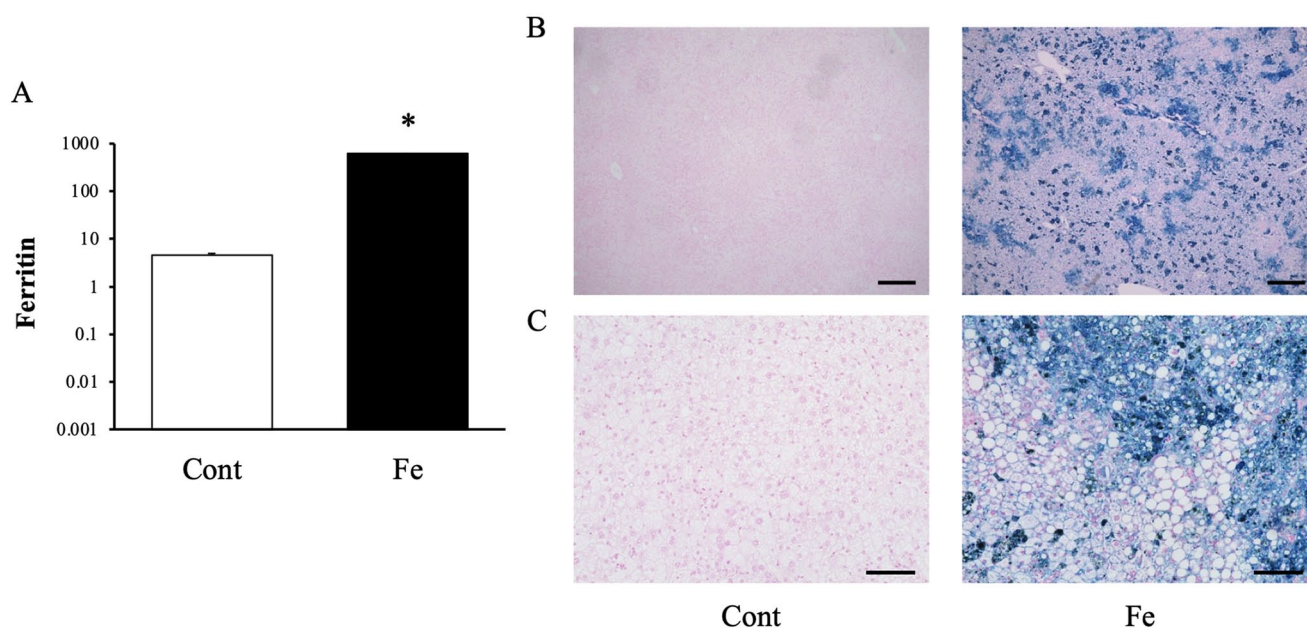


**Figure 3.** Iron metabolism. (A) The serum ferritin levels. (B) and (C) Berlin blue staining in the liver (B: scale bar=400µm, C: scale bar=100µm). All data are shown as the mean value ± SE; n=5 in both groups. SE: standard error. \*P<0.05 vs Cont group.

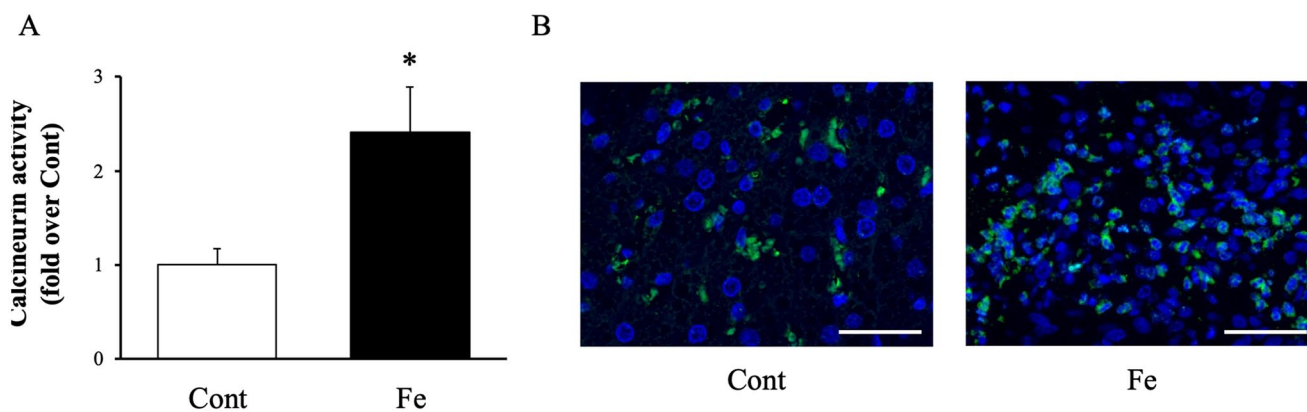


**Figure 4.** Calcineurin activity and immunofluorescence staining of TFEB in the liver. (A) Hepatic calcineurin activity. (B) The nuclear translocation expression levels of TFEB (scale bar=50µm). All data are shown as the mean value ± SE; n=5 in both groups. TFEB: transcription factor EB; SE: standard error. \*P<0.05 vs Cont group.

monocyte chemotactic protein 1 (*MCP1*) and tumor necrosis factor- $\alpha$  (*TNF- $\alpha$* ), were significantly upregulated in the Fe group (Figure 5(C)).

### Expression of genes related to lysosome membrane and autophagy

In the liver, the mRNA expression of lysosome-related genes, including lysosome-associated membrane protein 2 (*LAMP2*), transient receptor potential cation channel, mucolipin subfamily, member 1 (*TRPML1*), and CLN3 lysosomal/endosomal transmembrane protein, battenin (*CLN3*), was significantly upregulated in the Fe group compared to those in the Cont group (Figure 6(A)). The mRNA expression of autophagy-related genes, including unc-51 like autophagy activating kinase 1 (*ULK1*,

UV radiation resistance-associated gene (*UVRAG*), and autophagy-related gene 14 (*ATG14*), was upregulated in the Fe group (Figure 6(B)). In addition, the mRNA expression of nuclear receptor co-activator 4 (*NCOA4*), a ferritinophagy cargo receptor, and members of the RAS oncogene family (*Rab10*) and dynamin 2 (*DNM2*), lipophagy cargo receptors, was also upregulated in the Fe group (Figure 6(C) and (D)).

### Ferroptosis analysis

Immunofluorescence staining showed that the 4-HNE level markedly increased in the Fe group compared to that in the Cont group (Figure 7(A)). Quantitative analysis using ImageJ also showed that the fluorescent area was significantly higher in the Fe group than in the Cont group (Figure 7(B)).

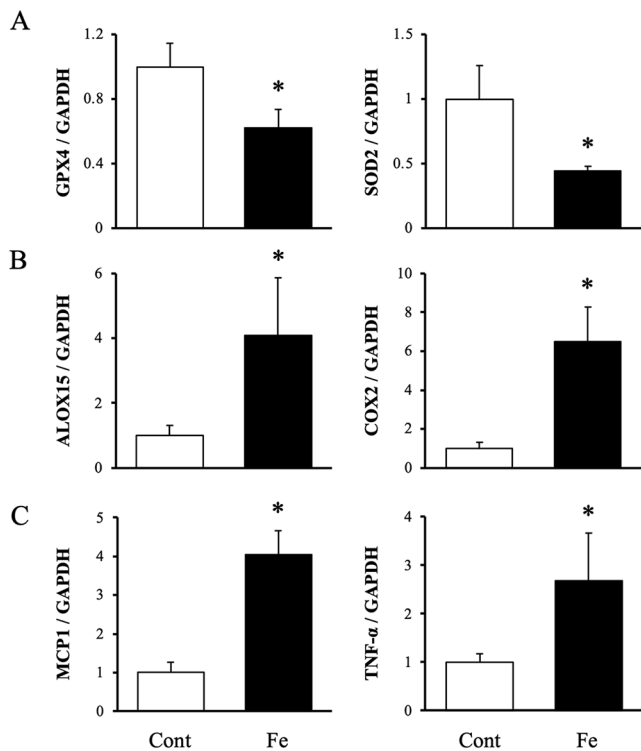


**Figure 5.** Quantitative RT-PCR analysis of oxidative stress- and inflammation-related genes in the liver. (A) mRNA levels of antioxidative response enzymes *GPX4* and *SOD2*. (B) mRNA levels of oxidative response enzymes *ALOX15* and *COX2*. (C) mRNA levels of inflammation markers *MCP1* and *TNF-α*. *GAPDH* was used as the internal standard for (A) to (C). All data are shown as the mean value  $\pm$  SE;  $n=5$  in both groups.

*GPX4*: glutathione peroxidase 4; *SOD2*: superoxide dismutase 2; *ALOX15*: arachidonate 15-lipoxygenase; *COX2*: cyclooxygenase 2; *MCP1*: monocyte chemoattractant protein 1; *TNF-α*: tumor necrosis factor- $\alpha$ ; *GAPDH*: glyceraldehyde 3-phosphate dehydrogenase; SE: standard error.

\* $P < 0.05$  vs Cont group.

Transmission electron microscopy (TEM) revealed significant mitochondrial contraction in the Fe group compared to that in the Cont group (Figure 7(C) and (D)).

## Discussion

NASH has a worldwide prevalence of approximately 12%, and its progression to cirrhosis and hepatocellular carcinoma represents a serious health concern.<sup>25</sup> However, the mechanism of disease progression and exacerbating factors remain unclear. In this study, we focused on iron overload in NASH pathology. Iron is an essential trace element for almost all living organisms. However, iron overload results in increased reactive oxygen species (ROS) production, which causes cell dysfunction or death, tissue damage, and disease.<sup>26,27</sup> In addition, iron overload induces ferroptosis, an iron-dependent novel form of cell death and is associated with the progression of NASH pathology.<sup>6,8</sup> Recent studies have shown that ferroptosis is closely related to autophagy, especially ferritinophagy and lipophagy, two types of selective autophagy.<sup>14,15</sup> Autophagy is a self-degradative intracellular process that degrades abnormal proteins and over-abundant or damaged organelles. During autophagy, cellular components are ingested into double-membrane vesicles, known as autophagosomes, and degraded by lysosomes. Autophagy

occurs via non-selective or selective pathways. The selective pathway (selective autophagy) mediates the recycling of specific organelles, such as mitochondria, nuclei, lysosomes, lipid droplets (LDs), and ferritin. Based on the target of degradation, selective autophagy is classified as follows: mitophagy (mitochondria), nucleophagy (nuclei), lysophagy (lysosome), lipophagy (LDs), and ferritinophagy (ferritin).<sup>28</sup> The activation of autophagy is critical for cell survival and tissue homeostasis; however, the degradation products of autophagy may have adverse effects.<sup>14,15</sup> Ferritinophagy and lipophagy are examples of selective autophagy that induce ferroptosis.

In this study, the Cont and Fe groups with NAS scores  $>5$  were defined as NASH. The NAS scores were not significantly different between the two groups; however, lobular inflammation and Ishak fibrosis stage were significantly higher in the Fe group than those in the Cont group. In addition, the Fe group presented with iron overload; increased accumulation of iron in the liver; elevated serum iron, ferritin, TIBC, and TSAT levels; and decreased transferrin levels (Figure 2(B) and (C) and Figure 3(A to C) and Table 2). As the total food intake was regulated such that it was equal in the two groups (Figure 1(A)), these results suggest that iron overload aggravated NASH. The relationship between selective autophagy and ferroptosis in the process of NASH exacerbation caused by iron overload is presented in the schematic model in Figure 8.

Iron overload causes ROS generation and increases the uptake of intracellular calcium ions.<sup>29</sup> The increase in calcium ions activates calcineurin, a protein phosphatase.<sup>30,31</sup> Activation of calcineurin results in the dephosphorylation of TFEB (an autophagy-promoting factor) in the cytosol and its subsequent translocation into the nucleus.<sup>32</sup> Nuclear TFEB upregulates the expression of lysosome- and autophagy-related genes by binding to Coordinated Lysosomal Expression and Regulation (CLEAR) sequences, which are common in many lysosome-related genes in hepatic cells.<sup>32–35</sup> As shown in Figure 5(A) and (B), oxidative stress was upregulated following iron overload. In addition, calcineurin activity increased, and TFEB migrated into the nucleus in the Fe group, which is consistent with the results of previous studies. The mRNA expression of lysosome- (*LAMP2*, *TRPML1*, and *CLN3*) and autophagy-related (*ULK1*, *UVRAG*, and *ATG14*) genes was significantly upregulated in the Fe group compared to that in the Cont group (Figure 6(A) and (B)), suggesting that nuclear translocation of TFEB promoted autophagy.

In the alternate pathway, iron overload increases ferritin, a protein that stores excessive iron as a non-toxic complex. The ferritin complex plays an important role in maintaining iron homeostasis via degradation to produce  $Fe^{2+}$  during iron overload as well as during iron deficiency.<sup>36,37</sup> The degradation of ferritin by autophagy is known as ferritinophagy, a type of selective autophagy. NCOA4 plays an important role in iron homeostasis by regulating ferritin storage/release and is a selective cargo receptor that mediates ferritinophagy. The serum ferritin levels in the Fe group were higher than those in the Cont group (Figure 3(A)). In addition, the mRNA expression of *NCOA4* was significantly upregulated in the Fe group compared with that in the

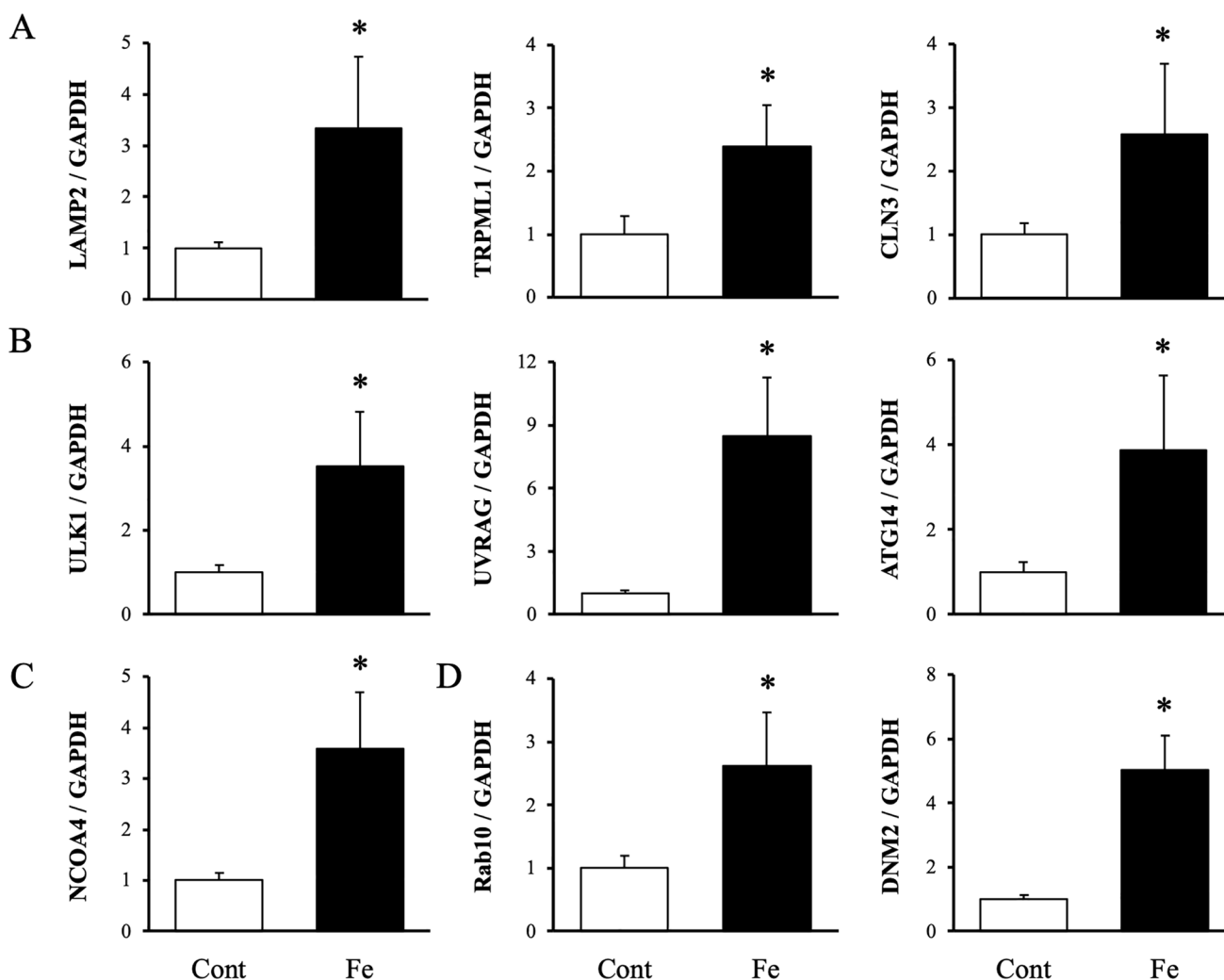


**Figure 6.** Quantitative RT-PCR analysis of lysosome and autophagy-related genes in the liver. (A) mRNA levels of lysosome-related genes *LAMP2*, *TRPML1*, and *CLN3*. (B) mRNA levels of autophagy-related genes *ULK1*, *UVRAG*, and *ATG14*. (C) mRNA levels of ferritinophagy cargo receptor *NCOA4*. (D) mRNA levels of lipophagy cargo receptors *Rab10* and *DNM2*. *GAPDH* was used as the internal standard for (A) to (D). All data are shown as the mean value  $\pm$  SE;  $n=5$  in both groups.

RT-PCR: quantitative reverse transcription polymerase chain reaction; *LAMP2*: lysosome-associated membrane protein 2; *TRPML1*: transient receptor potential cation channel, mucopolin subfamily, member 1; *CLN3*: CLN3 lysosomal/endosomal transmembrane protein, battenin; *ULK1*: unc-51 like autophagy activating kinase 1; *UVRAG*: UV radiation resistance-associated gene; *ATG14*: autophagy-related gene 14; *NCOA4*, nuclear receptor co-activator 4; *Rab10*: member of the RAS oncogene family; *DNM2*: dynamin 2; *GAPDH*: glyceraldehyde 3-phosphate dehydrogenase; SE: standard error.

\* $P < 0.05$  vs Cont group.

Cont group, suggesting that iron overload promoted ferritinophagy. Fratta Pasini *et al.*<sup>38</sup> demonstrated that excess ferritin is degraded by *NCOA4*-mediated ferritinophagy, which is consistent with our experimental results. Moreover, it is suggested that ferritinophagy was also accelerated by an autophagy mechanism via the nuclear translocation of TFEB.

We previously reported that SHRSP5/Dmcr rats fed an HFC diet accumulate LDs (TG) in hepatic cells.<sup>39,40</sup> Excess TG in the hepatic cells is degraded by the lipase pathway and also by lipophagy.<sup>41–43</sup> Lipophagy is selective autophagy mechanism that specifically degrades LDs and plays an essential role in LD homeostasis. The mRNA expression of *Rab10* and *DNM2*, selective cargo receptors that mediate lipophagy,<sup>44</sup> was significantly upregulated in the Fe group compared to that in the Cont group (Figure 6(D)), suggesting that TFEB accelerates lipophagy during iron overload. These results suggest that iron overload elevates both ferritinophagy and lipophagy.

Ferroptosis, an iron-dependent form of cell death, is caused by the accumulation of lipid hydroperoxides that promote the oxidation of membrane lipids and damage the lipid bilayer of the cell membrane.<sup>6</sup> Excessive oxidative stress and lipid peroxidation promote ferroptosis.<sup>45,46</sup> The morphological characteristics of ferroptosis include mitochondrial contraction, increased membrane density, and decreased mitochondrial cristae.<sup>6</sup> In this study, the Fe group showed increased accumulation of 4-HNE and contraction of mitochondria compared to the Cont group. In addition, the mRNA expression of *GPX4*, an indicator of ferroptosis, was lower in the Fe group than in the Cont group, suggesting that iron overload enhanced ferroptosis in hepatic cells. In recent years, the relationship between ferroptosis and selective autophagy, including ferritinophagy and lipophagy, has been reported.<sup>14,15</sup> Ferritinophagy is a pathway that degrades ferritin to produce  $Fe^{2+}$ , which is used in the mitochondria for ATP production. However, excess



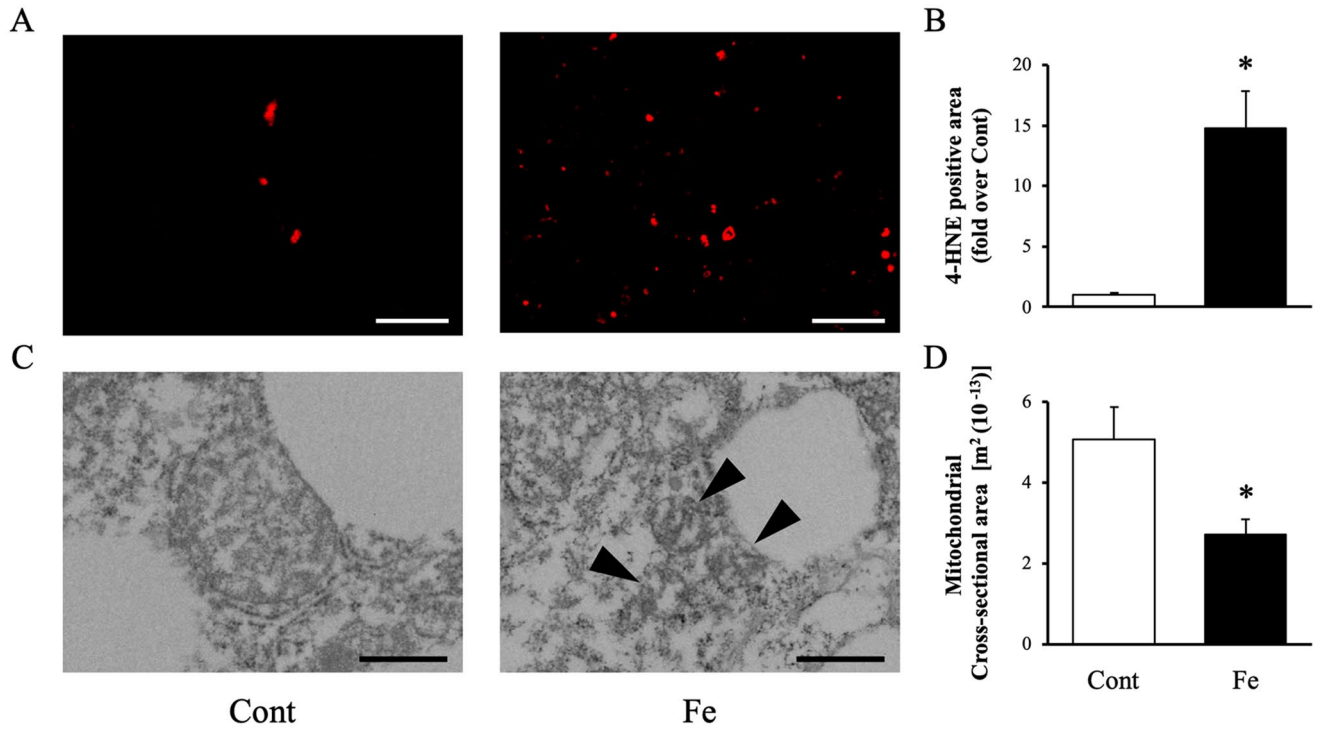


**Figure 7.** Immunofluorescence staining of 4-HNE and TEM images in the liver. (A) Deposition levels of 4-HNE in the liver (scale bar=50 μm). (B) 4-HNE deposition rate in the liver. (C) TEM images of mitochondria in the liver. Black arrows show mitochondria (scale bar=500 nm). (D) The mitochondrial cross-sectional area in the liver. A total of 20 mitochondria per group were examined. All data are shown as the mean value ± SE; n=5 in both groups. 4-HNE: 4-hydroxynonenal; TEM: transmission electron microscopy; SE: standard error. \*P<0.05 vs Cont group.

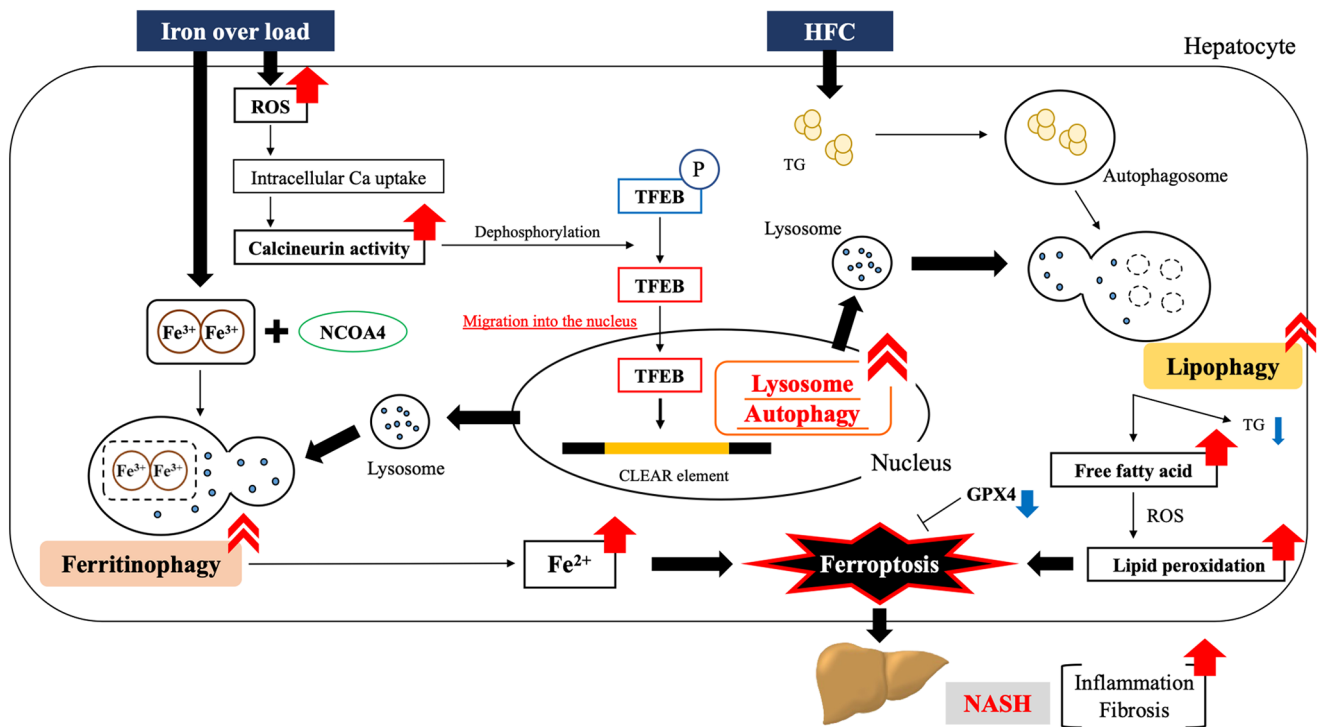


**Figure 8.** Mechanism of iron overload induces ferroptosis via selective autophagy and aggravates NASH in SHRSP5/Dmcr rats. NASH: non-alcoholic steatohepatitis.

Fe<sup>2+</sup> catalyzes the Fenton reaction, which reduces hydrogen peroxide to produce hydroxyl radicals, a type of ROS. As

reported previously, this pathway occurs not only during iron deficiency but also during iron overload.<sup>37,38</sup> Increased

levels of hydroxyl radicals generate oxidative stress and promote ferroptosis. Several studies have reported that ferritinophagy induces ferroptosis.<sup>47–49</sup> In this study, ferritinophagy was promoted in the Fe group compared to the Cont group, suggesting that ferroptosis was accelerated by ferritinophagy. LDs are degraded during lipophagy to produce FFAs.<sup>43</sup> FFAs are non-esterified fatty acids (FAs) transported throughout the body via blood circulation for use as an energy source in various tissues in the body. FAs are classified according to the number of double bonds as follows: no double bonds=saturated fatty acids, one double bond=monounsaturated fatty acids, and two or more double bonds=polyunsaturated fatty acids (PUFAs). PUFAs are unstable because they contain many unsaturated double bonds and are readily oxidized to lipid peroxidation by ROS. The accumulation of lipid peroxidation, produced by the oxidation of PUFA, in cell membranes promotes ferroptosis.<sup>50</sup> Bai *et al.*<sup>15</sup> reported that lipophagy promotes ferroptosis. Consistent with these reports, FFA and ROS were upregulated in the Fe group compared to that in the Cont group (Table 2 and Figure 5(A) and (B)), suggesting that lipophagy promotes ferroptosis.

Focusing on hepatic stellate cells (HSCs) and macrophages, it is unclear whether excess iron directly activates HSCs and macrophages. Mehta *et al.* evaluated the effects of excess iron on fibrogenesis and transforming growth factor (TGF)-beta signaling in mouse HSCs. As a result, HSCs expressed the iron uptake protein transferrin receptor 1 and the iron transport protein ferroportin, and iron activated the TGF-beta pathway and collagen secretion in HSCs. Iron chelators (deferrioxamine (DFO)) can inhibit these activities. Therefore, HSCs express iron transport proteins, and excess iron may directly activate HSCs via the TGF-beta pathway.<sup>51</sup> In addition, iron determines the fate and function of M1 macrophages, especially during cell development and differentiation.<sup>52</sup> Iron overload increases M1 marker levels such as interleukin (IL)-6, TNF- $\alpha$ , and IL-1 $\beta$  and decreases M2 markers such as transglutaminase 2 (TGM2), that is, promotes polarization toward M1 macrophages.

A limitation of this study is that we only demonstrated an association between the exacerbated NASH phenotype and altered autophagy and ferroptosis but not a causal relationship for the role of increased ferroptosis in exacerbating the NASH phenotype. However, evidence suggests that ferroptosis mediates iron overload in the NASH phenotype.<sup>53</sup> Various inhibitors of the ferroptosis pathway, such as rosiglitazone, vitamin E, Fer-1, Lip-1, and DFO, may exert protective effects against NASH in both *in vitro* and *in vivo* experiments. In particular, chelating agents such as DFO or deferiprone, which are used to remove excess iron from the body, are inhibitors of the ferritinophagy–ferroptosis pathway. In fact, deferiprone inhibited necrotic cell death, inflammatory cell infiltration, and inflammatory cytokine expression in an NASH animal model.<sup>8</sup> Therefore, inhibition of the ferritinophagy–ferroptosis pathway may have protective effects against NASH with iron overload in *in vitro* or *in vivo* experiments. In addition, it is unknown whether hepatocyte-derived factors corresponding to iron overload can stimulate macrophage activation. However, to the best of our knowledge, high mobility group box 1 (HMGB1) released by cells undergoing ferroptosis may be one factor that activates phagocytosis and the mobilization

of macrophages. Ferroptotic cells that release HMGB1 induce inflammation and macrophage recruitment by activating molecular inflammatory pathways.<sup>54</sup>

Thus, our results suggest that ferritinophagy and lipophagy synergize to promote ferroptosis. In conclusion, NASH is aggravated by ferroptosis, which is enhanced by ferritinophagy and lipophagy under conditions of iron overload.

#### AUTHOR CONTRIBUTIONS

KH contributed to the data analysis, formal analysis, investigation, visualization, and writing – original draft. SK contributed to the data analysis and investigation. HN contributed to the data analysis and investigation. TF contributed to the data analysis and investigation. TO contributed to the data analysis and investigation. KK contributed to the data analysis and investigation. IS contributed to the data analysis and investigation. SH contributed to the supervision and writing – review and editing. MF contributed to the data analysis and investigation. SY contributed to the supervision and writing – review and editing. SR contributed to the data analysis and investigation. SW contributed to the conceptualization, funding acquisition, project administration, and writing – review and editing.


#### DECLARATION OF CONFLICTING INTERESTS

The author(s) declared no potential conflicts of interest with respect to the research, authorship, and/or publication of this article.

#### FUNDING

The author(s) disclosed receipt of the following financial support for the research, authorship, and/or publication of this article: This work was supported by grants from the Japan Society for the Promotion (grant no. 15K191780) and Grant-in-Aid for Scientific Research (C) (grant no. 18K10993) to S.W., Grant-in-Aid for Scientific Research (A) (grant no. 20H00548) to S.H., and Grant-in-Aid for Early-Career Scientists (grant no. 23K16796) to I.S.

#### ORCID ID

Shogo Watanabe  <https://orcid.org/0000-0002-1700-2892>

#### SUPPLEMENTAL MATERIAL

Supplemental material for this article is available online.

#### REFERENCES

1. Younossi ZM, Koenig AB, Abdelatif D, Fazel Y, Henry L, Wymer M. Global epidemiology of nonalcoholic fatty liver disease—meta-analytic assessment of prevalence, incidence, and outcomes. *Hepatology* 2016;64:73–84
2. Nd AM. Non-alcoholic fatty liver disease, an overview. *Integr Med* 2019;18:42–9
3. Kowdley KV, Belt P, Wilson LA, Yeh MM, Neuschwander-Tetri BA, Chalasani N, Sanyal AJ, Nelson JE; NASH Clinical Research Network. Serum ferritin is an independent predictor of histologic severity and advanced fibrosis in patients with nonalcoholic fatty liver disease. *Hepatology* 2012;55:77–85
4. Manne V, Handa P, Kowdley KV. Pathophysiology of nonalcoholic fatty liver disease/nonalcoholic steatohepatitis. *Clin Liver Dis* 2018;22:23–37
5. Marmur J, Beshara S, Eggertsen G, Onelöv L, Albiin N, Danielsson O, Hultcrantz R, Stål P. Hepcidin levels correlate to liver iron content, but

- not steatohepatitis, in non-alcoholic fatty liver disease. *BMC Gastroenterol* 2018;**18**:78
6. Dixon SJ, Lemberg KM, Lamprecht MR, Skouta R, Zaitsev EM, Gleason CE, Patel DN, Bauer AJ, Cantley AM, Yang WS, Morrison B 3rd, Stockwell BR. Ferroptosis: an iron-dependent form of nonapoptotic cell death. *Cell* 2012;**149**:1060–72
  7. Li J, Cao F, Yin HL, Huang ZJ, Lin ZT, Mao N, Sun B, Wang G. Ferroptosis: past, present and future. *Cell Death Dis* 2020;**11**:88
  8. Tsurusaki S, Tsuchiya Y, Koumura T, Nakasone M, Sakamoto T, Matsuo M, Imai H, Yuet-Yin Kok C, Okochi H, Nakano H, Miyajima A, Tanaka M. Hepatic ferroptosis plays an important role as the trigger for initiating inflammation in nonalcoholic steatohepatitis. *Cell Death Dis* 2019;**10**:449
  9. Kroemer G, Mariño G, Levine B. Autophagy and the integrated stress response. *Mol Cell* 2010;**40**:280–93
  10. Mizushima N, Komatsu M. Autophagy: renovation of cells and tissues. *Cell* 2011;**147**:728–41
  11. Feng Y, He D, Yao Z, Klionsky DJ. The machinery of macroautophagy. *Cell Res* 2014;**24**:24–41
  12. Kraft C, Reggiori F, Peter M. Selective types of autophagy in yeast. *Biochim Biophys Acta* 2009;**1793**:1404–12
  13. Khaminets A, Behl C, Dikic I. Ubiquitin-dependent and independent signals in selective autophagy. *Trends Cell Biol* 2016;**26**:6–16
  14. Li N, Wang W, Zhou H, Wu Q, Duan M, Liu C, Wu H, Deng W, Shen D, Tang Q. Ferritinophagy-mediated ferroptosis is involved in sepsis-induced cardiac injury. *Free Radic Biol Med* 2020;**160**:303–18
  15. Bai Y, Meng L, Han L, Jia Y, Zhao Y, Gao H, Kang R, Wang X, Tang D, Dai E. Lipid storage and lipophagy regulates ferroptosis. *Biochem Biophys Res Commun* 2019;**508**:997–1003
  16. Kitamori K, Naito H, Tamada H, Kobayashi M, Miyazawa D, Yasui Y, Sonoda K, Tsuchikura S, Yasui N, Ikeda K, Moriya T, Yamori Y, Nakajima T. Development of novel rat model for high-fat and high-cholesterol diet-induced steatohepatitis and severe fibrosis progression in SHRSP5/Dmcr. *Environ Health Prev Med* 2012;**17**:173–82
  17. Horai Y, Utsumi H, Ono Y, Kishimoto T, Ono Y, Fukunari A. Pathological characterization and morphometric analysis of hepatic lesions in SHRSP5/Dmcr, an experimental non-alcoholic steatohepatitis model, induced by high-fat and high-cholesterol diet. *Int J Exp Pathol* 2016;**97**:75–85
  18. Kleiner DE, Brunt EM, Van Natta M, Behling C, Contos MJ, Cummings OW, Ferrell LD, Liu YC, Torbenson MS, Unalp-Arida A, Yeh M, McCullough AJ, Sanyal AJ; Nonalcoholic Steatohepatitis Clinical Research Network. Design and validation of a histological scoring system for nonalcoholic fatty liver disease. *Hepatology* 2005;**41**:1313–21
  19. Elias J Jr, Altun E, Zacks S, Armao DM, Woosley JT, Semelka RC. MRI findings in nonalcoholic steatohepatitis: correlation with histopathology and clinical staging. *Magn Reson Imaging* 2009;**27**:976–87
  20. Ishak K, Baptista A, Bianchi L, Callea F, De Groote J, Gudat F, Denk H, Desmet V, Korb G, MacSween RN, Phillips MJ, Portmann BG, Poulsen H, Scheuer PJ, Schmid M, Thaler H. Histological grading and staging of chronic hepatitis. *J Hepatol* 1995;**22**:696–9
  21. Goodman ZD. Grading and staging systems for inflammation and fibrosis in chronic liver diseases. *J Hepatol* 2007;**47**:598–607
  22. Fruman DA, Pai SY, Klee CB, Burakoff SJ, Bierer BE. Measurement of calcineurin phosphatase activity in cell extracts. *Methods* 1996;**9**:146–54
  23. Esterbauer H, Benedetti A, Lang J, Fulceri R, Fauler G, Comporti M. Studies on the mechanism of formation of 4-hydroxynonenal during microsomal lipid peroxidation. *Biochim Biophys Acta* 1986;**876**:154–66
  24. Tsikas D. Assessment of lipid peroxidation by measuring malondialdehyde (MDA) and relatives in biological samples: analytical and biological challenges. *Anal Biochem* 2017;**524**:13–30
  25. Williams CD, Stengel J, Asike MI, Torres DM, Shaw J, Contreras M, Landt CL, Harrison SA. Prevalence of nonalcoholic fatty liver disease and nonalcoholic steatohepatitis among a largely middle-aged population utilizing ultrasound and liver biopsy: a prospective study. *Gastroenterology* 2011;**140**:124–31
  26. Tian Q, Qin B, Gu Y, Zhou L, Chen S, Zhang S, Zhang S, Han Q, Liu Y, Wu X. ROS-mediated necroptosis is involved in iron overload-induced osteoblastic cell death. *Oxid Med Cell Longev* 2020;**2020**:1295382
  27. Dixon SJ, Stockwell BR. The role of iron and reactive oxygen species in cell death. *Nat Chem Biol* 2014;**10**:9–17
  28. Gatica D, Lahiri V, Klionsky DJ. Cargo recognition and degradation by selective autophagy. *Nat Cell Biol* 2018;**20**:233–42
  29. Nakamura K, Miura D, Kusano KF, Fujimoto Y, Sumita-Yoshikawa W, Fuke S, Nishii N, Nagase S, Hata Y, Morita H, Matsubara H, Ohe T, Ito H. 4-Hydroxy-2-nonenal induces calcium overload via the generation of reactive oxygen species in isolated rat cardiac myocytes. *J Card Fail* 2009;**15**:709–16
  30. Klee CB, Crouch TH, Krinks MH. Calcineurin: a calcium- and calmodulin-binding protein of the nervous system. *Proc Natl Acad Sci U S A* 1979;**76**:6270–3
  31. Rusnak F, Mertz P. Calcineurin: form and function. *Physiol Rev* 2000;**80**:1483–521
  32. Medina DL, Di Paola S, Peluso I, Armani A, De Stefani D, Venditti R, Montefusco S, Scotto-Rosato A, Prezioso C, Forrester A, Settembre C, Wang W, Gao Q, Xu H, Sandri M, Rizzuto R, De Matteis MA, Ballabio A. Lysosomal calcium signalling regulates autophagy through calcineurin and TFEB. *Nat Cell Biol* 2015;**17**:288–99
  33. Sardiello M, Palmieri M, di Ronza A, Medina DL, Valenza M, Gennarino VA, Di Malta C, Donaudy F, Embrione V, Polishchuk RS, Banfi S, Parenti G, Cattaneo E, Ballabio A. A gene network regulating lysosomal biogenesis and function. *Science* 2009;**325**:473–7
  34. Palmieri M, Impey S, Kang H, di Ronza A, Pelz C, Sardiello M, Ballabio A. Characterization of the CLEAR network reveals an integrated control of cellular clearance pathways. *Hum Mol Genet* 2011;**20**:3852–66
  35. Settembre C, Di Malta C, Polito VA, Garcia Arencibia M, Vetrini F, Erdin S, Erdin SU, Huynh T, Medina D, Colella P, Sardiello M, Rubinsztein DC, Ballabio A. TFEB links autophagy to lysosomal biogenesis. *Science* 2011;**332**:1429–33
  36. Kidane TZ, Sauble E, Linder MC. Release of iron from ferritin requires lysosomal activity. *Am J Physiol Cell Physiol* 2006;**291**:C445–55
  37. Asano T, Komatsu M, Yamaguchi-Iwai Y, Ishikawa F, Mizushima N, Iwai K. Distinct mechanisms of ferritin delivery to lysosomes in iron-depleted and iron-replete cells. *Mol Cell Biol* 2011;**31**:2040–52
  38. Fratta Pasini AM, Stranieri C, Girelli D, Busti F, Cominacini L. Is ferroptosis a key component of the process leading to multiorgan damage in COVID-19? *Antioxidants* 2021;**10**:1677
  39. Watanabe S, Kumazaki S, Kusunoki K, Inoue T, Maeda Y, Usui S, Shinohata R, Ohtsuki T, Hirohata S, Kusachi S, Kitamori K, Mori M, Yamori Y, Oka H. A high-fat and high-cholesterol diet induces cardiac fibrosis, vascular endothelial, and left ventricular diastolic dysfunction in SHRSP5/Dmcr rats. *J Atheroscler Thromb* 2018;**25**:439–53
  40. Watanabe S, Kumazaki S, Yamamoto S, Sato I, Kitamori K, Mori M, Yamori Y, Hirohata S. Non-alcoholic steatohepatitis aggravates nitric oxide synthase inhibition-induced arteriosclerosis in SHRSP5/Dmcr rat model. *Int J Exp Pathol* 2018;**99**:282–94
  41. Sathyanarayan A, Mashek MT, Mashek DG. ATGL promotes autophagy/lipophagy via SIRT1 to control hepatic lipid droplet catabolism. *Cell Rep* 2017;**19**:1–9
  42. Singh R, Kaushik S, Wang Y, Xiang Y, Novak I, Komatsu M, Tanaka K, Cuervo AM, Czaja MJ. Autophagy regulates lipid metabolism. *Nature* 2009;**458**:1131–5
  43. Singh R, Cuervo AM. Lipophagy: connecting autophagy and lipid metabolism. *Int J Cell Biol* 2012;**2012**:282041
  44. Li Z, Schulze RJ, Weller SG, Krueger EW, Schott MB, Zhang X, Casey CA, Liu J, Stöckli J, James DE, McNiven MA. A novel Rab10-EHBP1-EHD2 complex essential for the autophagic engulfment of lipid droplets. *Sci Adv* 2016;**2**:e1601470
  45. Park MW, Cha HW, Kim J, Kim JH, Yang H, Yoon S, Boonpraman N, Yi SS, Yoo ID, Moon JS. NOX4 promotes ferroptosis of astrocytes by oxidative stress-induced lipid peroxidation via the impairment of mitochondrial metabolism in Alzheimer's diseases. *Redox Biol* 2021;**41**:101947
  46. Stockwell BR, Friedmann Angeli JP, Bayir H, Bush AI, Conrad M, Dixon SJ, Fulda S, Gascón S, Hatzios SK, Kagan VE, Noel K, Jiang X, Linkermann A, Murphy ME, Overholtzer M, Oyagi A, Pagnussat GC, Park J, Ran Q, Rosenfeld CS, Salnikow K, Tang D, Torti FM, Torti SV, Toyokuni S, Woerpel KA, Zhang DD. Ferroptosis: a regulated cell death nexus linking metabolism, redox biology, and disease. *Cell* 2017;**171**:273–85

47. Gao M, Monian P, Pan Q, Zhang W, Xiang J, Jiang X. Ferroptosis is an autophagic cell death process. *Cell Res* 2016;**26**:1021–32
48. Bauckman KA, Mysorekar IU. Ferritinophagy drives uropathogenic *Escherichia coli* persistence in bladder epithelial cells. *Autophagy* 2016;**12**:850–63
49. Hou W, Xie Y, Song X, Sun X, Lotze MT, Zeh HJ 3rd, Kang R, Tang D. Autophagy promotes ferroptosis by degradation of ferritin. *Autophagy* 2016;**12**:1425–8
50. Yang WS, Kim KJ, Gaschler MM, Patel M, Shchepinov MS, Stockwell BR. Peroxidation of polyunsaturated fatty acids by lipoxygenases drives ferroptosis. *Proc Natl Acad Sci U S A* 2016;**113**:E4966–75
51. Mehta KJ, Coombes JD, Briones-Orta M, Manka PP, Williams R, Patel VB, Syn WK. Iron enhances hepatic fibrogenesis and activates transforming growth factor- $\beta$  signaling in murine hepatic stellate cells. *Am J Med Sci* 2018;**355**:183–90
52. Yang Y, Wang Y, Guo L, Gao W, Tang TL, Yan M. Interaction between macrophages and ferroptosis. *Cell Death Dis* 2022;**13**:355
53. Zhang H, Zhang E, Hu H. Role of ferroptosis in non-alcoholic fatty liver disease and its implications for therapeutic strategies. *Biomedicines* 2021;**9**:1660
54. Luo X, Gong HB, Gao HY, Wu YP, Sun WY, Li ZQ, Wang G, Liu B, Liang L, Kurihara H, Duan WJ, Li YF, He RR. Oxygenated phosphatidylethanolamine navigates phagocytosis of ferroptotic cells by interacting with TLR2. *Cell Death Differ* 2021;**28**:1971–89

(Received February 1, 2023, Accepted May 18, 2023)